Bragg reflection waveguide diode lasers

Bhavin J. Bijlani and Amr S. Helmy*

Edward S. Rogers Sr. Department of Electrical and Computer Engineering, University of Toronto, 10 King's College Road, Toronto, Ontario M5S3G4, Canada
**Corresponding author: a.helmy@utoronto.ca*

Received August 7, 2009; revised October 19, 2009; accepted November 3, 2009; posted November 5, 2009 (Doc. ID 115464); published November 30, 2009

What we believe to be the first demonstration of an edge-emitting Bragg reflection waveguide laser is reported. The laser utilized InGaAs quantum wells emitting at 980 nm, with $Al_xGa_{1-x}As$ core and claddings. The lasing mode is centered in a low-index core with a width of 700 nm, hence providing a large mode volume with strong discrimination against any modes other than the fundamental photonic bandgap mode. Single-transverse mode operation is observed with thresholds as low as 157 A/cm^2. The propagation losses of the mode were measured for the first time and found to be 11.4 cm^{-1}. © 2009 Optical Society of America

OCIS codes: 130.5296, 140.5960, 230.1480.

Bragg reflection waveguides (BRWs) have attracted increasing interest recently for various applications. These include nonlinear optics [1], dispersion engineering [2,3], slow light [4], and novel laser designs [5,6]. First proposed in detail by Yeh and Yariv in 1976 [7], a BRW is essentially a one-dimensional (1D) photonic bandgap (PBG) structure with a line-defect serving as a waveguide core. The core layer is surrounded on both sides by transverse Bragg reflectors (TBRs), suitably designed to reflect the modal transverse wavevector and confine the field in the core region, which can be a low-index medium such as air.

The benefits of lasers operating in the BRW mode have been studied theoretically in the past. For example, it has been shown that large mode volumes are possible for large core sizes, while still maintaining a single-mode behavior [5]. This can result in high power output as the photon density is reduced resulting in decreased filamentation and spectral hole burning. It has also been noted that modes formed through transverse resonance, such as those in BRWs, can have higher gain coefficients compared to their conventional counterparts [8]. Modes arising from PBG structures also possess strong mode discrimination, allowing for stable single mode operation. This is due to large mode spacing and the significant losses of higher-order modes [9,10].

A single-sided BRW double-heterostructure laser was first demonstrated in 1978 by Shellan *et al.* [11]. There have also been several demonstrations of two-dimensional (2D) PBG-guided diode lasers [6,10]. Impediments for the wide use of 2D PBG-guided lasers include the carrier loss to the recombination on the etched surfaces, the excessive light scattering, and the challenging fabrication involved. These rendered optical pumping as the preferred injection scheme for 2D PBG-guided lasers. In addition, traditional 2D air-hole PBG line-defect waveguides use a high-index core such as Si. This will result in total internal reflection (TIR) modes being present in the core. As heating takes place during operation, the core index increases and raises the possibility of light coupling into and, hence, lasing in TIR modes instead of the PBG mode. By guiding in a low-index medium, this problem is circumvented. To the best of our knowledge, this Letter is the first demonstration of a double-sided 1D BRW laser with a low-index core.

Recently, we have shown that similar BRW structures can be used for highly efficient phase-matching of ultrafast second-order optical nonlinearities [1]. As such, another significance of this class of lasers is its potential for monolithic integration with elements where $\chi^{(2)}$ processes can be efficiently utilized. This would enable a new class of optoelectronic integrated circuits, where ultrafast parametric processes can be used to realize devices such as monolithic electrically injected optical parametric oscillators or electrically injected entangled photon-pair sources.

The wafer was grown using metal–organic chemical vapor deposition on a 3°-off [001] n-type GaAs substrate. The reflector layers were $Al_xGa_{1-x}As$ with $x=0$ and 0.30 for the high and low refractive index layers, respectively. The core material is $x=0.37$, rendering the core the lowest refractive index in the waveguide, which ensures that it cannot sustain a TIR mode. Two $In_{0.2}Ga_{0.8}As$ quantum wells emitting at 980 nm were used, and the structure was capped with 50 nm of GaAs. The core layer thickness d_{core} was chosen to be 700 nm, which is significantly larger than typical laser structures operating at similar wavelengths. The PBG mode that ensures maximum confinement of the field in the core takes place at the center of the stop band of the Bragg reflectors. This point requires that the stack is a quarter-wave to the transverse k-vector component of the mode [1].

The effective modal index of this quarter-wave BRW can be found by $n_{\text{eff}}=\sqrt{n_{\text{core}}^2-\lambda^2/2d_{\text{core}}^2}$ [2]. Here, λ is the free-space wavelength. Utilizing this equation, $n_{\text{eff}}=3.199$ for the PBG mode. Applying the quarter-wave condition on the TBR then sets the high, n_1, and low, n_2, index stack layer thicknesses of 167 and 281 nm, respectively. The BRW used eight Bragg periods above and below the core, giving a total structure thickness of approximately 8 μm. The refractive index profile of the fabricated structure is shown in Fig. 1(a). The effective index is indicated by the dashed line. It is evident that this value is lower than any of the material indices, a distinct feature of

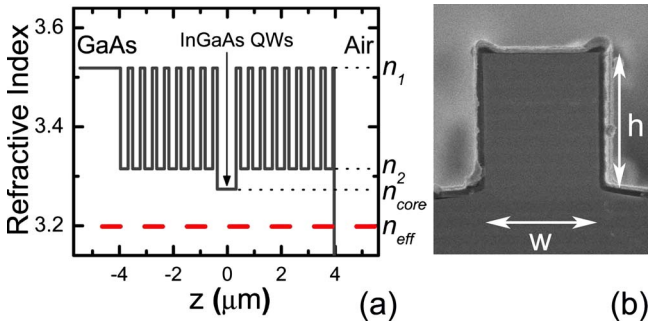

Fig. 1. (Color online) (a) Refractive index profile of the structure. The effective index of the PBG mode is indicated by a dashed line. (b) SEM micrograph of a ridge laser cross section. The etch depth is $h=3.6$ μm, and the ridge width is $w=3.2$ μm.

PBG modes. It should also be noted that this laser structure is identical to that of a vertical cavity surface emitting laser. However, in the case discussed here, the Bragg stacks are designed to be a quarter-wave for the transverse wavevector and not the full wavevector. The n-type stack was doped with carbon, while the p-type stack was doped with silicon. All interfaces were linearly graded in composition over 25 nm to reduce electrical resistance. The core had a center region of 220 nm that was intentionally undoped, while a region of 240 nm on either side of this center region, adjacent to the stacks, was lightly doped.

Theoretical values for the mode leakage, α_{leakage}, of the PBG mode were computed using a complex root-finding algorithm based on the transfer matrix method. For the structure reported here, $\alpha_{\text{leakage}}=0.5$ cm^{-1}. This value has been confirmed through other techniques [12]. Utilizing the transverse resonance condition [3], the next highest-order even PBG mode (second order) has $n_{\text{eff}}=2.605$ and $\alpha_{\text{leakage}}=1008$ cm^{-1}. This demonstrates the significant mode discrimination of this class of lasers.

Samples were coated with 400 nm plasma-enhanced chemical vapor deposition (PECVD) SiO_2; then lines of 3 μm width were defined with photolithography and transferred into the silica mask using CHF_3 inductively coupled plasma (ICP) etching. Ridge waveguides with a depth of 3.6 μm were etched into the AlGaAs via $BCl_3/Cl_2/Ar$ ICP. After removing the etch mask, 200 nm PECVD SiO_2 was deposited and an oxide opening was patterned and etched. Electrical contacts were deposited using electron-beam evaporation and individual laser-diode bars were cleaved to different lengths. A scanning electron microscope (SEM) cross section of the laser structure can be seen in Fig. 1(b). The diodes were tested with uncoated facets.

To characterize the laser, a 7 mm diameter silicon PIN photodiode was brought to less than 500 μm of the facet to monitor the output power. The proximity of the detector and its large detection area ensured that all the power was measured. The heat sink was maintained at a temperature of 20°C. Typical light-current-voltage (*LIV*) curves are shown in Fig. 2. For the laser which had a length of 580 μm, the turn-on

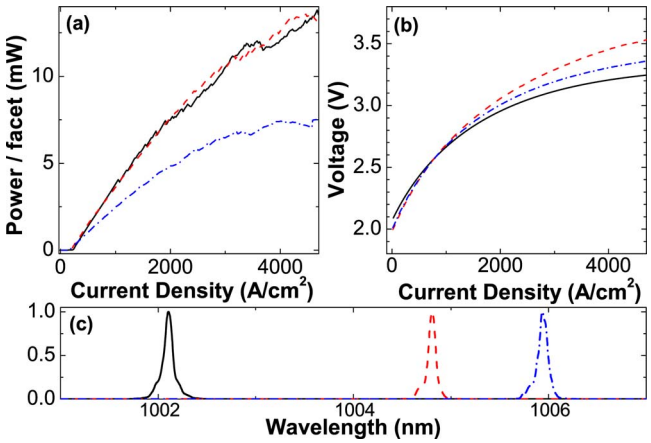

Fig. 2. (Color online) (a) *LI* curves for lasers of 500 μm (solid curve), 580 μm (dashed curve), and 970 μm (dashed-dotted curve) cavity lengths. Threshold for the 580 μm laser is 5.4 mA or 231 A/cm^2 assuming 4 μm lateral width. (b) *IV* curves for the same lasers. (c) Spectra at currents 2.5× (solid curve), 5× (dashed curve), and 8× (dashed-dotted curve) above threshold.

voltage was 2.2 V and the threshold current density was 231 A/cm^2. The longest cavity length tested was 970 μm, and it exhibited the lowest measured current density for the wafer at 157 A/cm^2.

At current densities lower than 20× threshold, heating effects have not hampered the device operation. Spectrally, the laser emission exhibits only one transverse mode. This can be seen in Fig. 2(c), where spectra are taken at 2.5×, 5×, and 8× the threshold current value. The wavelength redshifts at a rate of about 0.1 nm/mA due to carrier induced effects. The onset of thermal rollover takes place at approximately 20× threshold.

In order to verify that the laser is operating in the PBG mode, near-field (NF) and far-field (FF) were examined and compared with theory. To obtain the NF profile, a 60× microscope objective was used. The theoretical calculation, illustrated in Fig. 3(a), can be compared with the obtained images shown in Fig. 3(b). The two profiles are qualitatively similar. In the center, a bright peak is evident, with adjacent peaks above and below that are separated by nodes. Further peaks and nodes are evident but less pronounced owing to the limitations of the optics and camera dynamic range.

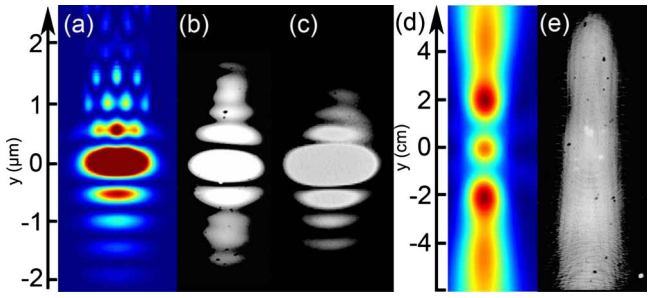

Fig. 3. (Color online) (a) Computed NF profile of the PBG mode. (b) Measured NF profile just above threshold, (c) at 50× threshold. (d) Computed planar FF and (e) measured planar FF image at about 5 mm from the facet.

A FF is typically represented in terms of the angle from the source. However, to facilitate the characterization of the extremely divergent PBG mode, planar FFs were used for comparison. The planar FF was captured by bringing the camera as close as 5 mm from the laser facet while minimizing the camera gain. A typical FF profile is shown in Fig. 3(f) with the theoretical planar FF profile in Fig. 3(e) calculated at a distance of 5 mm. Both NF and FF were computed using a full-vectorial commercial mode solver [13]. Theory and experiment show vertical beams, albeit the fine features seen in Fig. 3(d), could not be resolved in the measurement. This is likely due to saturation and finite dynamic range effects in the camera. Nonetheless, the similarities in NF and FF provide convincing evidence that lasing is taking place in the PBG mode.

The NF and FF profiles were not found to change in shape at current densities as high as 50× threshold. This is achieved thanks to the high losses of the higher-order PBG mode and by designing out the competing TIR modes. This is evident in Fig. 3(c).

Spectral analysis of subthreshold spectra can elucidate valuable information about the laser [14]. Through this technique the group index, the modal loss, and the laser transparency current density can be determined. A sample subthreshold spectrum, which was taken using a high-resolution spectrometer (8 pm resolution), is shown in the inset of Fig. 4. The group index found from the peak spacing is 3.89. The cavity propagation gain/loss K at different subthreshold currents can be obtained through the fitting of such a spectrum as shown in Fig. 4. The current at which $K=0$ on this curve is the transparency current density. This point is found to be at a value of 35 A/cm^2. Theoretical predictions suggest that PBG modes can possess enhanced spontaneous emission factors [15], thus reducing threshold and transparency current densities. The lasers discussed represent a practical vehicle, where these effects can be experimentally investigated without complex fabrication processes.

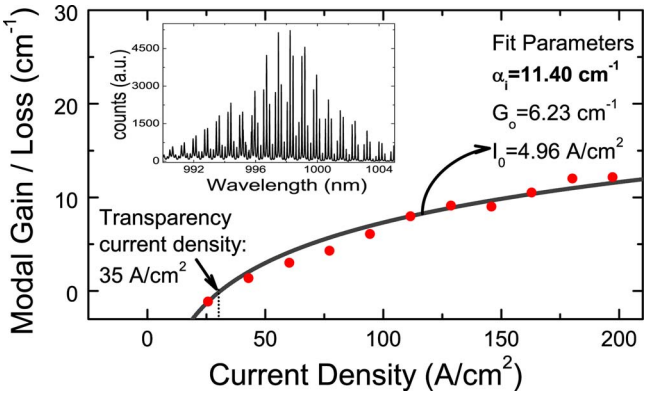

Fig. 4. (Color online) Modal propagation gain/loss versus current density, calculated from Fourier transform analysis of subthreshold spectra. The data (points) are fit (line) to the logarithmic equation in the text. (Inset) Subthreshold spectrum of a 580 μm BRW laser operating at 172 A/cm^2.

The cavity mode gain/loss data can be fit to the logarithmic relation: $K=G_0\ln(I/I_0)-\alpha_i$, which relates the current to the cavity mode gain/loss. From this fit a modal propagation loss of $\alpha_i=11.4$ cm^{-1} is obtained. The loss values were confirmed using an independent technique, which uses the dependence of the laser properties on the cavity length.

In summary, edge-emitting BRW laser-diodes were demonstrated and characterized. This design benefits from a strong mode discrimination to maintain single-transverse mode operation. The NF and FF both corroborate lasing in the PBG mode. Low thresholds, the lowest measured being 157 A/cm^2, and stable NF and FF emissions up to 50× threshold current were obtained. The BRW modal loss was measured to be 11.4 cm^{-1}, which is the first report for the propagation loss value for these modes. With proper design and engineering with second-order nonlinear devices, this laser can serve as novel platform for integrated parametric photonic devices.

This work was funded by the Natural Sciences and Engineering Research Council of Canada (NSERC). We acknowledge CMC Microsystems for the epitaxial growth.

References

1. P. Abolghasem, J. Han, B. Bijlani, and A. S. Helmy, Opt. Express **17**, 9460 (2009).
2. B. R. West and A. S. Helmy, Opt. Express **14**, 4073 (2006).
3. J. Li and K. S. Chiang, J. Opt. Soc. Am. B **24**, 1942 (2007).
4. A. Fuchida and F. Koyama, IEICE Electron. Express **5**, 349 (2008).
5. T. H. Her, Opt. Express **16**, 7197 (2008).
6. G. A. DeRose, L. Zhu, J. M. Choi, J. K. S. Poon, A. Yariv, and A. Scherer, J. Vac. Sci. Technol. B **24**, 2926 (2006).
7. P. Yeh and A. Yariv, Opt. Commun. **19**, 427 (1976).
8. A. Yariv, Y. Xu, and S. Mookherjea, Opt. Lett. **28**, 176 (2003).
9. L. Zhu, A. Scherer, and A. Yariv, IEEE J. Quantum Electron. **43**, 934 (2007).
10. A. Mock, L. Lu, E. H. Hwang, J. O'Brien, and P. D. Dapkus, IEEE J. Sel. Top. Quantum Electron. **15**, 892 (2009).
11. J. B. Shellan, W. Ng, A. Yariv, P. Yeh, and A. Cho, Opt. Lett. **2**, 136 (1978).
12. S. Dasgupta, A. Ghatak, and B. P. Pal, Opt. Commun. **279**, 83 (2007).
13. Lumerical Solutions, www.lumerical.com.
14. D. Hofstetter and R. L. Thornton, IEEE J. Quantum Electron. **34**, 1914 (1998).
15. J. P. Dowling and C. M. Bowden, Phys. Rev. A **46**, 612 (1992).